

1 Introduction

We describe an information-gathering approach for exploring an unknown scene using a range sensor. Our explorer maintains a map of known and likely obstacles, under an Ising-like prior distribution, and follows a greedy best-next-view policy, whereby uncertainty at the next timestep is minimized by maximizing the uncertainty of the next range measurement. Uncertainty is efficiently approximated by a novel Poisson disk sampling technique. Our algorithm improves the performance of recent visibility-based planning approaches that come with guaranteed performance bounds on the expected path length to complete exploration, and extends them to allow exploration of an unbounded region.

2 Prior Work

Information-driven visual exploration has a long history, both for the case of eye movement and for the more general case of full mobility. The former is relevant to visual attention and oculomotor control, where saccadic motions are hypothesized to be related to the uncertainty on the irradiance in different locations of the visual field. Information gain (uncertainty reduction) occurs due to the uneven distribution of sensing elements in the retina (foveal vision). Since we are interested in uniformly-sampled omnidirectional sensors, customary in robotics applications, no information gain can occur as a result of gaze control. Therefore, we focus on the case of parallax motion (translation of the optical center), where uncertainty is due to *occlusions* as well as *scaling* phenomena that can be reduced by control of the vantage point. The use of information-theoretic criteria for visual exploration dates back to the literature on Active Vision (?, ?, ?, ?). For range sensors, where most of the uncertainty is due to occlusions, entropy can be related to visibility, and therefore several have adopted geometric criteria (?, ?, ?, ?, ?). Much of this work is concerned with a greedy approach to information maximization by seeking the “best next view” for a particular task, which could be recognition or manipulation (?, ?, ?). The problem is also addressed in the context of optimal control (?, ?), sequential decision ?, “Value of Information” ?, partially-observable path planning (?, ?), among others. In some cases, the problem exhibits submodular characteristics that make it amenable to be solved with efficient algorithms with provable guarantees ?. For instance ? perform underwater inspection, assuming a known map, exploiting submodular optimization. Unfortunately, our setting is not submodular, and therefore proper formalization in terms of optimal control or sequential decision processes would yield an intractable inference problem. As customary, therefore, we seek for surrogate criteria that yield algorithms with provable guarantees.

3 Information-Driven Exploration

In this chapter we consider the problem where the variable of interest is the geometry and topology of a two-dimensional scene (e.g. the map of a building) represented by an indicator function defined on a domain $\Omega \subseteq \mathbb{R}^2$, supported on a closed subset $\mathcal{O} \subseteq \Omega$ that describes unknown “obstacles” or “objects.” The explorer follows a continuous path $x(t)$ in the space $\Omega \setminus \mathcal{O}$. Let $\mathcal{A} \subseteq \Omega \setminus \mathcal{O}$ be the path-component of $\Omega \setminus \mathcal{O}$ containing $x(0)$.

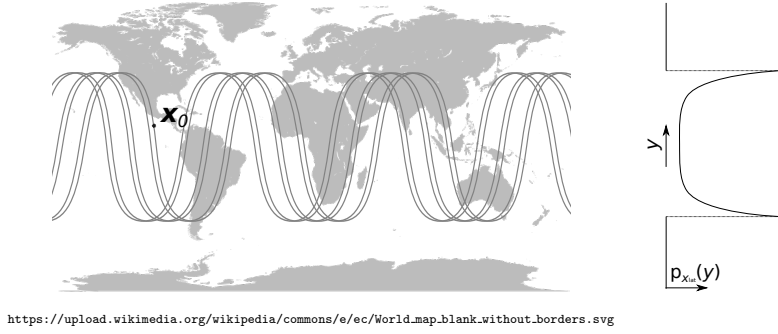


Figure 1: *Lost Astronaut Prior Distribution* The crash site $\mathbf{x}(t)$ is defined by a random time t , chosen uniformly in $[0, T]$. This induces prior marginal probabilities on the latitude and longitude of the crash site. The limiting distribution for as $T \rightarrow \infty$ is shown at right, while the limiting distribution on longitude is uniform.

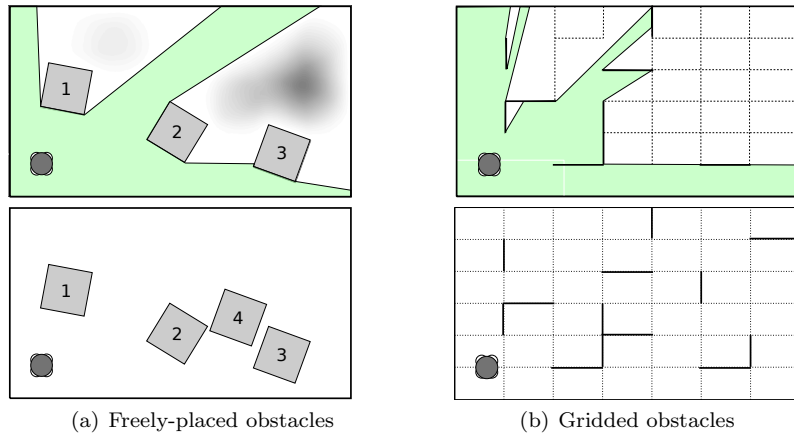


Figure 2: *Exploring a Random Room* (a) In the first case, the explorer knows that there are four identical boxes scattered within a room of known dimensions, three of which he can see. There is a “shadow region” where the disposition of space is not known. Based on allowable configurations of the missing block (blocks can not intersect, unseen blocks can not lie in known free space), the explorer can compute, at each point in the shadow region, the probability that that point is covered by an obstacle. (b) In the second case, partitions (black line segments), constrained to grid lines (dotted lines) divide up a room. Seeing any point of a grid segment reveals the disposition of any other point on that grid segment.

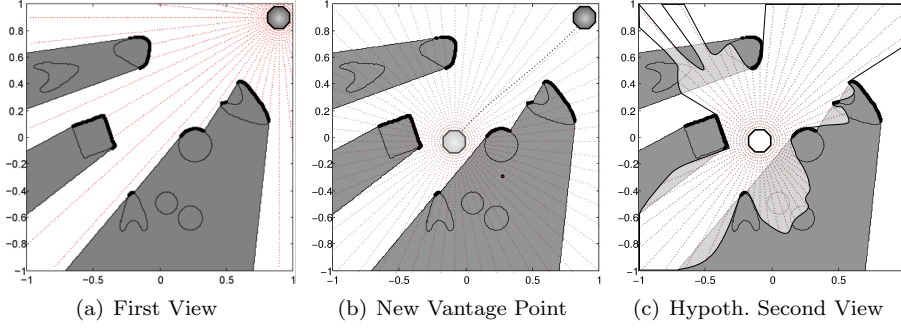


Figure 3: *Range Measurement Planning* An explorer

At discrete timesteps t_i , $i = 1, \dots, L$, the explorer at $x_i = x(t_i)$ measures an n -directional range map $\mathcal{Y}(x_i) \in (s\mathbb{N})^n$, which gives, to the nearest multiple of $s > 0$, the distance to the first obstacle along each sensor element’s line of sight. Let $\mathcal{Y}^t = \{\mathcal{Y}(x_i) : t_i < t\}$ denote the history of measurements up to time t .

Observe that each measurement is a function $\mathcal{Y}(x) = h(x, \Omega, \mathcal{O})$ of the scene (Ω, \mathcal{O}) and the vantage point x . If we interpret this as a realization of a stochastic process, each measurement \mathcal{Y}_i reduces the uncertainty in \mathcal{O} . Although each range sensor is affected by uncertainty due to scaling, spatial quantization, noise, etc. most of the uncertainty is due to occlusions, for objects are opaque and therefore at the outset we have no knowledge of the scene behind an occluder. An information-gathering controller then aims to design the control $\{u_j\}_{j=i}^L$ that maximizes the reduction in the entropy of \mathcal{O} . Here we will assume for simplicity that we can control the instantaneous velocity, so that $x_{i+1} = x_i + u_i$.

In order to compute the “information gain” of a measurement at time t , we have to define suitable distributions on the objects of interest. We maintain an estimate of the explorer’s state at time t as a distribution $\mathbb{P}_t[\cdot] = \mathbb{P}[\cdot | \mathcal{Y}^t]$ on possible realizations of \mathcal{A} .

4 Next-View Entropy

In order to compute the “information gain” of a measurement at time t , we have to define suitable distributions on the objects of interest. We maintain an estimate of the explorer’s state at time t as a distribution $\mathbb{P}_t[\cdot] = \mathbb{P}[\cdot | \mathcal{Y}^t]$ on possible realizations of \mathcal{A} . Let $\mathcal{A}_t = \{x \in \Omega : \mathbb{P}_t[x \in \mathcal{A}] = 1\}$, $\mathcal{O}_t = \{x \in \Omega : \mathbb{P}_t[x \in \mathcal{A}] = 0\}$, and $\mathcal{U}_t = x \setminus (\mathcal{A}_t \cup \mathcal{O}_t)$ be the points which at time t are known to be visible, known to be invisible, or unknown, respectively. Finally, let \mathcal{V}^t denote the set of points that are visible to the observer from point x_t .

4.1 Measurement Uncertainty

Let

$$G = \{g_{ij} := s i(\cos(2\pi j/n), \sin(2\pi j/n))\}_{j < n}^{i,j \in \mathbb{N}}$$

be a uniform radial grid, centered at the origin, with radial spacing s and angular spacing $2\pi/n$ (see Figure 3). Although we define $\mathcal{Y}(x) = h(x, \Omega, \mathcal{O})$ as an $s\mathbb{N}$ -valued random n -tuple, it is natural to define an “alter-ego” $\mathcal{Y}_G(x)$, a Boolean-

valued random vector indexed by sample points $g_{ij} \in G$, with the constraint that

$$\mathcal{Y}_G(x)_{ij} = 0 \implies \mathcal{Y}_G(x)_{i+1,j} = 0.\text{\footnotemark}\quad (1)$$

Let $\mathcal{Y}(x)_{ij} = 1$ iff the point $g_{ij} + x$ is visible from x . Observe that

$$\mathcal{Y}_G(x)_{ij} = \mathbb{1}\{\mathcal{Y}(x)_j < s_i\}.$$

This defines a bijective relation between $\mathcal{Y}_G(x)$ and $\mathcal{Y}(x)$, so $\mathbb{H}_t[\mathcal{Y}_G(x)] = \mathbb{H}_t[\mathcal{Y}(x)]$.

Our next-view energy $E_t(x)$ is the expected decrease in uncertainty at time t , due to a measurement $\mathcal{Y}(x)$:

$$\begin{aligned} E_t(x) &:= \mathbb{E}_t[\mathbb{H}_t[\mathcal{O}] - \mathbb{H}_t[\mathcal{O}|\mathcal{Y}(x)]] = \mathbb{E}_t[\mathbb{H}_t[\mathcal{Y}(x)]] \\ &= \mathbb{H}_t[\mathcal{Y}(x)] = \mathbb{H}_t[\mathcal{Y}_G(x)]. \end{aligned}$$

We can decompose the latter into a sum of relative entropies, given a ordering g_{o_1}, g_{o_2}, \dots on G that respects radial ordering (i.e. if $o_k = (i, j)$, $o_\ell = (i', j')$, and $i' < i$, then $\ell < k$):

$$= \sum_k \mathbb{H}_t[\mathcal{Y}_G(x)_{o_k} | \{\mathcal{Y}_G(x)_{o_\ell}\}_{\ell < k}].$$

Now, if $\mathcal{Y}_G(x)_{i',j} = 0$ for $i' < i$, then by (1), we know $\mathcal{Y}(x)_{i,j}$ must equal 0 as well. In that case, the relative entropy at g_{ij} is zero, and so

$$\begin{aligned} &= \sum_{o_k=(i,j)} \underbrace{\mathbb{P}_t[\mathcal{Y}_G(x)_{i',j} = 1 \text{ for all } i' < i]}_{\text{Probability that } x + g_{ij} \text{ is visible from } x} \\ &\quad \cdot \underbrace{\mathbb{H}_t[\mathcal{Y}_G(x)_{o_k} | \{\mathcal{Y}_G(x)_{o_\ell}\}_{\ell < k}, \mathcal{Y}_G(x)_{i',j} = 1 \text{ for all } i' < i]}_{\text{Value of revealing scene at } x + g_{ij}}. \quad (2) \end{aligned}$$

Here, we will reference the first term through its complement, which we will call the “extinction probability”.

4.1.1 Extinction Probability

Define a normalized, instantaneous “mean free path” function $\text{MFP} : \Omega \rightarrow [0, \infty)$, such that for any curve $C \subseteq \Omega$,

$$\mathbb{P}_t[C \in \mathcal{A}] = \exp\left(\int_C \frac{\log(\mathbb{P}_t(x + g_{ij} \in \mathcal{A}))}{\text{MFP}(y)} |dy|\right).$$

Now we compute extinction probability, using a posterior estimate of the scene

$$\begin{aligned} \mathbb{P}_t[\mathcal{Y}_G(x)_{ij} = 1 | \mathcal{Y}_G(x)_{i-1,j} = 1] &= \exp\left(\int_{\text{line}(x+g_{i-1,j}, x+g_{ij})} \frac{\log(\mathbb{P}_t(x + g_{ij} \in \mathcal{A}))}{\text{MFP}(y)} |dy|\right) \\ &\approx \mathbb{P}_t(x + g_{ij} \in \mathcal{A})^{s/\text{MFP}(x+g_{ij})}, \end{aligned}$$

Induction on this chain of conditional probabilities gives

$$\mathbb{P}_t[\mathcal{Y}_G(x)_{ij} = 1] \approx \prod_{i' < i} \mathbb{P}_t(x + g_{i',j} \in \mathcal{A})^{s/\text{MFP}(x+g_{i',j})}$$

¹This formalizes the notion that a visible object blocks the view of objects further along its line of sight.

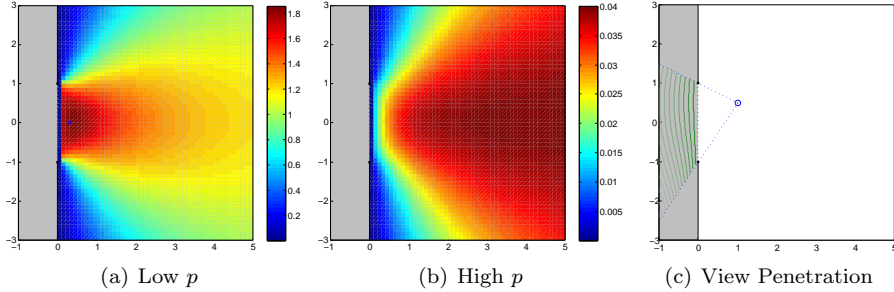


Figure 4: *Looking into a Closet with Uniform Obstacle Density* (a)-(b) Here we show the value of different vantage points for looking into an unexplored closet, for various values of p (MFP fixed). As p increases, a line of sight is less and less likely to penetrate deeply into the room, so the best vantage points move further back where lines of sight are more oblique. (c) Green lines show the probability-0.5 penetration limits of the blue explorer, for different values of p . As $p \rightarrow 1$, the depth of penetration near a point $u \in \partial\mathcal{U}^t$ becomes proportional to the cosine of the incidence angle between $\vec{n}(u)$ and the line of sight.

4.1.2 View Value

The second term in (2) is a conditional entropy whose computation is only tractable in certain limited situations. We will discuss these in the next section.

5 Obstacle Models

5.1 Uniform Obstacle Density

The simplest obstacle model assigns, to all points in \mathcal{U}^t , equal and nonzero probability p of lying in an obstacle. Additionally, it treats each sampled point as independent of all others. Thus the difficult entropy term in (2) reduces to a Bernoulli entropy:

$$\begin{aligned} \mathbb{H}_t[\mathcal{Y}_G(x)_{o_k=(i,j)} \mid \{\mathcal{Y}_G(x)_{o_\ell} \mid \ell < k\}, \mathcal{Y}_G(x)_{i'j} = 1 \text{ for all } i' < i] &= \mathbb{H}_t[\mathcal{Y}_G(x)_k] \\ &= -p \log p - (1-p) \log p, \end{aligned}$$

where we take $0 \log 0$ as 0. Additionally, we treat MFP(y) as constant. define

$$E_t(x) = \sum_{ij} (-p_{ij} \log p_{ij} - (1-p_{ij}) \log(1-p_{ij})) \prod_{i' < i} p_{i'j}^{s/\text{MFP}}, \quad (3)$$

where

$$p_{i,j} = \begin{cases} 0 & \text{line}(x + g_{i-1,j}, x + g_{ij}) \cap \mathcal{O}^t \neq \emptyset \\ 1 & \text{o.w., } x + g_{ij} \in \mathcal{A}^t \\ p & \text{o.w.} \end{cases}.$$

The values p and MFP are model parameters.

5.1.1 Instant Extinction

A special case of uniform obstacle density, proposed by Valente et al. ?, this takes the limit as $p^s/\text{MFP} \rightarrow 0$. To make sense of this, we treat it as a sum over visible shadow boundaries.

$$E_t(x) = \int_{\partial U^t \cap V^t} (r - x) \cdot \vec{n}(r) |dr|,$$

where $\vec{n}(r)$ is the outward-facing normal to the shadow boundary at point r . This gives greatest value to viewpoints which look directly (not obliquely) onto long, faraway (all lines of sight looking onto a faraway object are nearly parallel) shadow boundaries. The advantage of this method is that it can be integrated over shadow boundaries, although it assigns undue value to thin shadow regions which are unlikely to reveal much about the scene.

5.1.2 Independent Cells

A more general approach models an unknown scene as a random partition of the \mathcal{D} , with each cell of that partition assigned a random “color” (designation of “object” or “free space”), independent of all other cells. Once a partition is known, all that remains is to learn the coloring. The information gain of sampling $S \subseteq \mathcal{D}$ of a randomly-colored, known partition is equal to the sum of the entropies of the colorings of all the cells sampled. Denote the probability that cell c is an obstacle by p_c . Then,

$$\begin{aligned} \mathbb{H}[\{\mathcal{Y}(x) : x \in S\}] &= \mathbb{H}[\{\mathcal{Y}(x) : x \in S\} | \mathcal{P}] \\ &= \sum_{c : c \cap S \neq \emptyset} -p_c \log p_c - (1 - p_c) \log p_c. \end{aligned}$$

For an *unknown* partition \mathcal{P} ,

$$\mathbb{H}[\mathcal{Y}(S)] = \mathbb{H}[\mathcal{Y}(S) | \mathcal{P}] + \mathbb{I}[\mathcal{P}; \mathcal{Y}(S)] \quad (4)$$

So we can express the view value as

$$\begin{aligned} \mathbb{H}[\mathcal{Y}_G(x)_{o_k=(i,j)} | \{\mathcal{Y}_G(x)_{o_\ell} | \ell < k\}, \mathcal{Y}_G(x)_{i'j} = 1 \text{ for all } i' < i] \\ = \mathbb{H}[\mathcal{Y}_G(x)_{o_k} | \mathcal{P}, \dots] + \mathbb{I}[\mathcal{P}; \mathcal{Y}_G(x)_{o_k} | \dots], \end{aligned}$$

where “...” abbreviates the conditioning expression on the LHS. To simplify this computation, we assume that

$$\mathbb{I}[\mathcal{P}; \mathcal{Y}_G(x)_{o_k} | \{\mathcal{Y}_G(x)_{o_\ell} | \ell < k\}, \mathcal{Y}_G(x)_{i'j} = 1 \text{ for all } i' < i],$$

i.e., the additional information regarding the partition \mathcal{P} that can be learned from revealing a sample at $x + g_{ij}$, after revealing all the samples that precede it, is negligible, or at least constant as i and j vary.

Thus, we compute view value at g_{ij} as an average, over many known partitions \mathcal{P} , of the coloring information gained by sampling at $x + g_{ij}$. If no preceding nodes have sampled from the same cell, the gain is $-p_c \log p_c - (1 - p_c) \log p_c$. Otherwise gain is zero. So computing marginal entropy amounts to computing the probability that a sample point will be the “first to find” the cell that it lies in.

If \mathcal{P} is selected from a translationally- and rotationally-invariant probability distribution, this is equal to the expectation of the reciprocal of the number of grid points sharing a cell with $x + g_{ij}$. This expectation depends only on the position of g_{ij} in the grid, and is radially symmetric, so we can write

$$E_t(x) \approx \prod_{i' < i} w_i H(\mathbb{P}_t[x + g_{i'j}]) \cdot \mathbb{P}_t[x + g_{i'j} \in \mathcal{A}]^{s/\text{MFP}(x+g_{i'j})} \quad (5)$$

where $H(p) := -p \log p - (1-p) \log(1-p)$ and

$$w_i = \mathbb{E} \left[\frac{1}{\#(G \cap \mathcal{P}^r(g_{i,1}))} \right]. \quad (6)$$

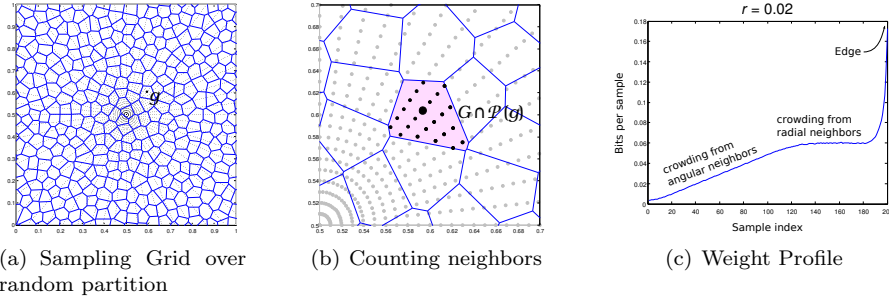


Figure 5: *Computing Sample Weights for a Radial Sampling Grid* **(a)** The weight w_{ij} is the expected energy gain from a sample at position $x + g_{ij}$ in $G(x)$. **(b)** The entropy of a sample from a random coloring of a random partition is taken as the expected value of the reciprocal of the number of samples with which it shares a cell (argument detailed in 5.2.4). **(c)** Since the sampling pattern G is radially symmetric, the weights w_{ij} can be described by a radial “profile”. The weight profile can be divided into three phases: The first phase, when nodes are likely to share cells with angular neighbors, shows an increase in weight as radius increases and radial neighbors get further and further away. The second phase, when angular neighbors are too far away to share cells, has constant weight. The third phase, as we reach the edge of the sampling pattern, shows a rapid doubling of weight, as nodes with many inner and outer (smaller or greater radius) neighbors give way to nodes with few or no outer neighbors.

5.2 Ising-Type Obstacles

A good obstacle model should incorporate assumptions about the shape, density and grouping behavior of obstacles. We have considered the obvious strategy of generating several hypothetical completions of partially revealed scenes, then averaging these completed scenes pointwise.

5.2.1 The Ising Model

We will define the Ising Model as a probability distribution $\mathcal{I}_{\mathcal{D}}$ on the set of binary, $\{-1, 1\}$ -valued images $\{I : \mathcal{D} \rightarrow \{-1, 1\}\}$, where \mathcal{D} is a 2- (or 3-) dimensional, 4- (or 6-) connected lattice \mathcal{D} (as shown in Fig. 5.2.2).

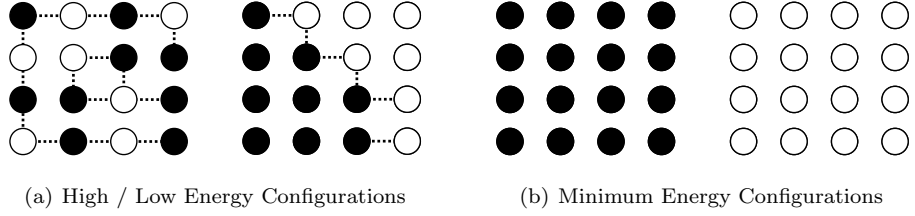


Figure 6: *Ising Model on a 4×4 Lattice* Likelihood under the Ising Model decreases exponentially with the number of edges between disagreeing nodes. Samples from the Ising Model are concentrated near the two minimum energy configurations: all-white or all-black.

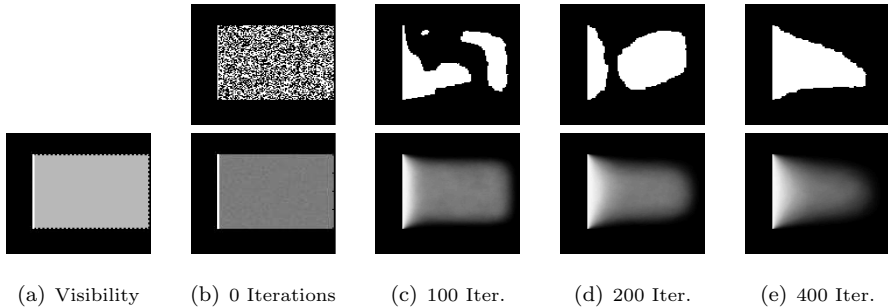


Figure 7: *Ising-type Obstacle Posterior* (a) The random process described in 5.2.2 is run on a scene with a rectangular shadow region (gray) produced by a flat obstacle edge (white). Black denotes known free space. (b)-(e) Top row: Images produced by the process. Bottom row: Average of 1000 runs.

$$P(I) \propto \exp(\beta(I_{ij}I_{i+1,j} + I_{ij}I_{i,j+1} + I_{ij}I_{i-1,j} + I_{ij}I_{i,j-1})) \quad (7)$$

5.2.2 Sampling from the Ising Model

To generate obstacle hypotheses, we run a Gibbs-sampling implementation of the subcritical Ising model (as discussed in ?), initialized with known obstacles, and halted after m iterations:

$$\mathbb{P}_t(I_{ij}^{m+1} = 1) = \begin{cases} \frac{\exp(-\beta(H_{ij}^m - 2))}{\exp(-\beta(H_{ij}^m - 2)) + \exp(-\beta(H_{ij}^m - 2))} & x_{ij} \in \mathcal{U}^t \\ 1 & x_{ij} \in \mathcal{A}^t \\ 0 & x_{ij} \in \mathcal{O}^t \end{cases} \quad (8)$$

with $H_{ij}^m := I_{i+1,j}^m + I_{ij}I_{i,j+1} + I_{ij}I_{i-1,j} + I_{ij}I_{i,j-1}$, and $\mathbb{P}_t(I_{ij}^0 = 1) = 0.5$ independently.

This defines a distribution $\mathcal{I}_{\mathcal{D}}^m$ on the set $\{I^m : \mathcal{D} \rightarrow \{0, 1\}\}$. Samples and statistics of this family of distributions are shown in Fig. 5.2.2

A good choice of the scale parameter m produces obstacles which “look like” (have similar thickness and curvature to) obstacles that the explorer is likely to see. The parameter can be estimated by estimating mean free path in the real

environment (e.g. by taking the average of the initial omni-directional range measurement) and choosing m to match. Figure 8 details how this is done.

Since these scenes are generated using a fixed coloring probability of 0.5, we normalize the MFP parameter so that $\mathbb{P}_t(y \in \mathcal{A})$ can vary:

$$\mathbb{P}_t[\mathcal{Y}_G(x)_{ij} = 0 \mid \mathcal{Y}_G(x)_{i-1,j} = 1] \approx \exp\left(\int_{\text{line}(x+g_{i-1,j}, x+g_{ij})} \frac{\log(\mathbb{P}_t(y \in \mathcal{A}))}{\log(0.5) \text{MFP}_{0.5}} dy\right)$$

5.2.3 Poisson-Disk Approximation

In order to express the viewpoint quality in Ising-type in a simple form like (5), we make use of certain statistical properties shared between our Ising-model scenes and randomly-colored partitions of uniformly-sized Voronoi cells. A Poisson-disc cover $\mathcal{P}^r \subseteq [-1, 1]^2$ is a uniformly random sampling of points in $[-1, 1]^2$ such that no two points have distance less than r , and no new point can be added without violating this property. These sample points induce a Voronoi partition $\mathcal{L}^r = \mathcal{L}(\mathcal{P}^r)$ of Ω . Random colorings ξ of these Voronoi partitions produce scenes I^r which bear a superficial resemblance to those produced by the Ising process, as seen in Figure 9

We have found that the Poisson-Voronoi random checkerboard is a useful surrogate for entropy computations involving Ising priors. For a given set of points $\{x_k\} \subseteq \Omega$, the entropy $\mathbb{H}[I^m(\{x_k\})]$ of sampling a random Ising scene I^m , with scale parameter m , can be estimated from the entropy $\mathbb{H}[IPV^r(\{x_k\})]$, for a random Poisson-Voronoi checkerboard. We have found a strong empirical correspondence between these joint entropies, for sampling sets of ten or fewer (estimating the distribution of the boolean random variable $I^m(\{x\})$, for a *single* sampling set $\{x\} \subseteq \Omega$ requires on the order of $2^{|\{x\}|}$ random Ising scenes - as we will see, it is much less taxing to generate the Poisson-Voronoi checkerboards). Correlations between these entropies, for a range of values of m and r , are plotted in Figure 13. Good matches are highlighted in pink.

5.2.4 Computing the Weights w_g

The statistical correspondence between Ising scenes and Voronoi checkerboards allows for the efficient computation of weights w_i . The joint entropy of samples from the random checkerboards is easily expressed as a weighted sum of the marginal entropies of the samples.

Recall that we can define

$$w_i = \mathbb{E}\left[\frac{1}{\#(G \cap \mathcal{P}^r(g))}\right]. \quad (9)$$

That is, G is the average of the reciprocal of the number of grid points in G that share a Voronoi cell with g , as determined by a random Poisson disk sampling (see Figure 9)

These weights can be computed numerically, for a given Poisson disk radius r and sampling pattern G , simply by generating many random Poisson-Voronoi partitions of the region surrounding G and averaging the reciprocal of the number of g 's neighbors in G . If the sampling pattern is radially symmetric, weights only depend on radial index. Weight profiles for several Poisson disk radii r are shown in Figure 5.

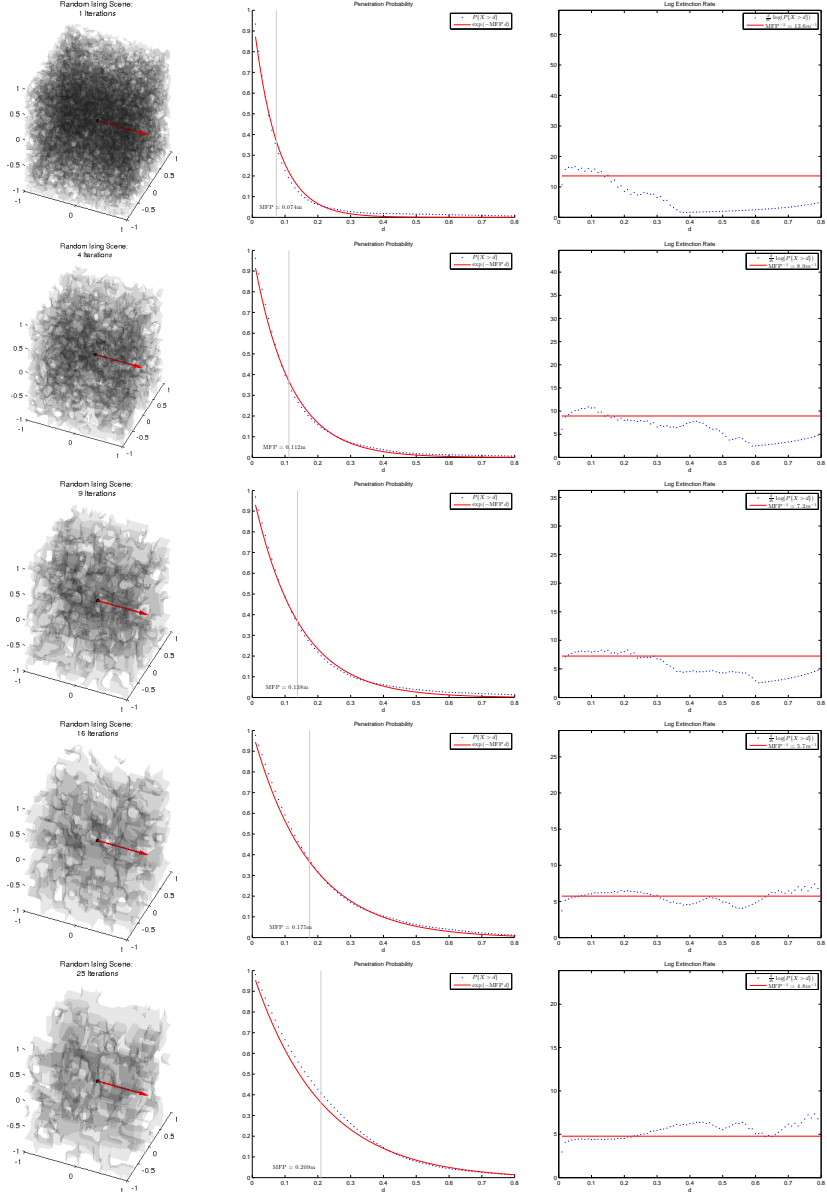


Figure 8: Extinction Profiles Here we show extinction profiles for Ising scenes with various granularities, indexed by number of update iterations. Instantaneous mean free path (derivative of log survival probability) and best-fit MFP are plotted together, showing that extinction in these scenes is well-modeled by an exponential decay.

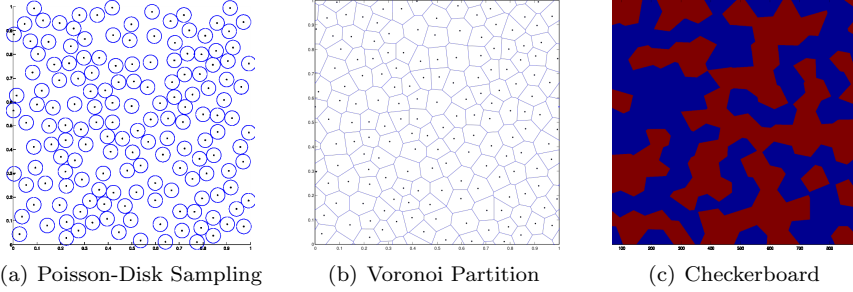


Figure 9: *Generating Poisson-Voronoi Checkerboard* (a) To produce a scene of desired granulation, we first produce a Poisson-Disc sampling of the domain, which gives a maximal set of points satisfying the property that the distance between two points is no less than r , a granularity parameter. (2) We compute a Voronoi partition of the scene based on that sampling (3) We color the cells independently, denoting them as obstacle or free space, with probability 1/2.

6 Numerical Optimizations

6.1 Bit-Parallel Monte Carlo

Recall that the update probability for our Monte Carlo Ising process is

$$P(I_{ij}^{t+1} = 1 | I^t) = \frac{\exp(\beta(H_{ij}^t - 2))}{\exp(\beta(H_{ij}^t - 2)) + \exp(-\beta(H_{ij}^t - 2))} \quad (10)$$

where

$$H_{ij}^t := I_{i+1,j}^t + I_{i,j+1}^t + I_{i-1,j}^t + I_{i,j-1}^t$$

This computation, which produces a single random bit, requires a new random floating-point number to be generated each time it is run. Many such bits need to be averaged to compute the marginal obstacle probabilities. If this operation could be approximated using only bit-wise operations, we could run these operations in parallel, one for each bit in a multi-bit datatype.

6.1.1 Overview

We define a random process \bar{I}_{ij}^t to approximate I_{ij}^t . For simplicity, \bar{I} will take values in $\{0, 1\}$, where I took values in $\{-1, 1\}$. First, we generate a random bit $B \sim \text{Bernoulli}(0.5)$. Recursively define

$$B^0 := B, \quad \text{and} \quad B^k := B_1^{k-1} \wedge B_2^{k-1}, \quad (11)$$

where $B_{1,2}^{k-1} \sim B^{k-1}$ are i.i.d. copies (their generation is discussed in the next section). Thus $B^k \sim \text{Bernoulli}(2^{-2^k})$. Define

$$\bar{I}_{ij}^{t+1} := \begin{cases} B(\bar{H}_{ij}^t) & \bar{H}_{ij}^t < 2 \\ \sim B(\bar{H}_{ij}^t) & \bar{H}_{ij}^t > 2 \\ B^0 & \bar{H}_{ij}^t = 2 \end{cases} \quad (12)$$

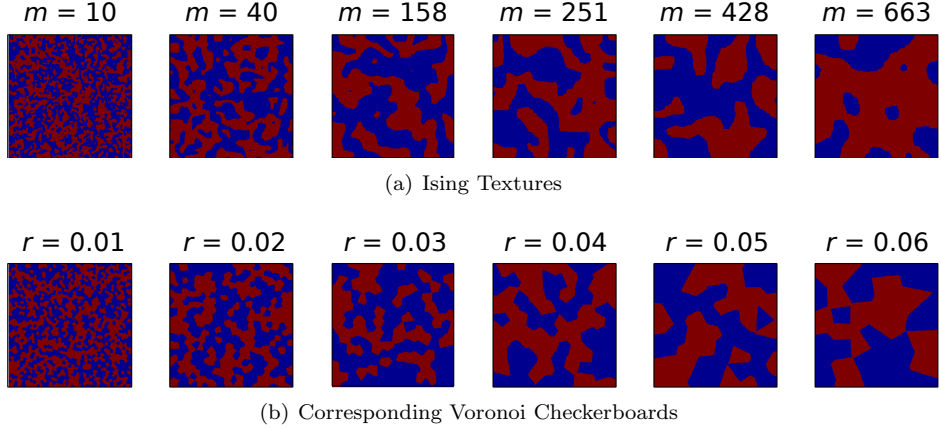


Figure 10: *Poisson-Voronoi Checkerboard* There is a superficial resemblance Ising-type obstacles and Voronoi checkerboards with appropriate scale parameters.

where

$$B(H) := \bigwedge_{k=1}^K ((\sim C_k(H)) \vee B^k), \quad (13)$$

$$C_k(H) := k\text{-th bit of } \bar{\beta}|H - 2| + 1. \quad (14)$$

Here $\bar{\beta}$ must be an integer. Observe that

$$\exp_2\left(-\sum_{k=1}^K 2^k C_k(H)\right) = 2^{-\bar{\beta}|H-2|-1},$$

and thus

$$E(\bar{I}_{ij}^{t+1}) = \begin{cases} 2^{-\bar{\beta}|H-2|-1} & H_{ij}^t < 2 \\ 1 - 2^{-\bar{\beta}|H-2|-1} & H_{ij}^t > 2 \\ 0.5 & H_{ij}^t = 2 \end{cases} \quad (15)$$

6.1.2 Computing the counts C_k

The counting bits C_k are computed as with a standard binary adder. This requires $O(k)$ bitwise AND and/or XOR operations for binary sum and carry, and about $2k$ boolean variables as registers.

6.1.3 Generating I.I.D. Bits

equivalent to the conjunction of 2^k independent coin-flips B_i^0 :

$$B^k \sim B_1^0 \wedge B_2^0 \wedge \cdots \wedge B_{2^k}^0.$$

Instead of calling the random number generator 2^k times, we generate a single N -bit ($N \geq 2^k$) integer L (for “long”), and conjoin it with k bit-shifted copies of itself. Recursively define

$$L^0 := L, \quad L^k := (L^{k-1} \wedge (L^{k-1} \ll 2^{k-1})) \ll 3 \cdot 2^{k-1} - 2. \quad (16)$$

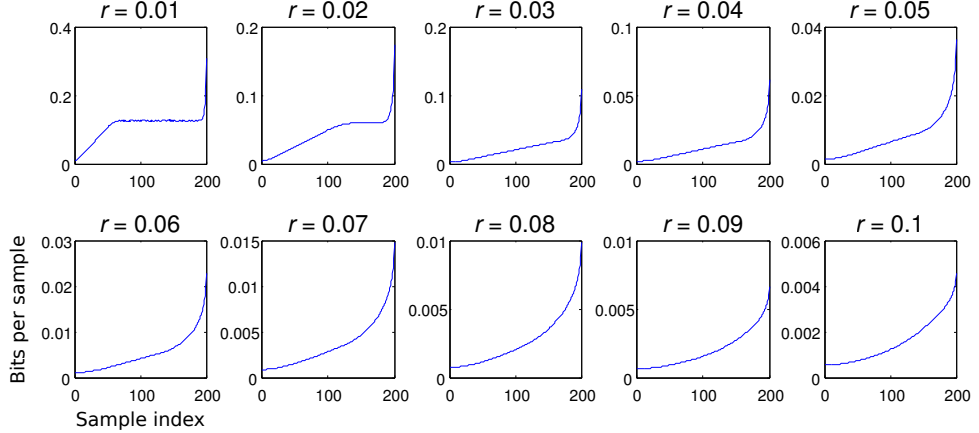


Figure 11: *2D Weight Profiles for Various r* Using the counting technique described in 5.1.2, we compute the information contribution, in bits, of samples at different (radial) positions on the radial sampling pattern (See Fig. 3), with regard to Poisson-Disc Voronoi scenes of various scales. In this case, we have 30 angular divisions and 200 radial divisions within a maximum radius of one unit.

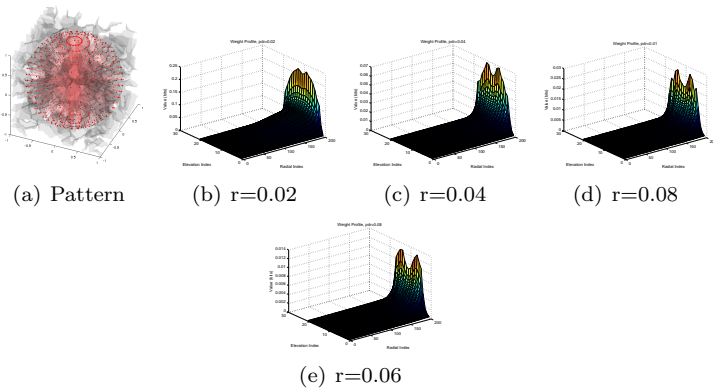


Figure 12: *3D Weight Profiles for Various r* The counting technique described in 5.1.2 is applied to 3D Poisson-Disc Voronoi Scenes, drawing from a spherical sampling pattern (a) with 30 azimuthal, 200 radial, and 11 elevation divisions. Again, radial symmetry around the vertical axis allows us to ignore azimuthal index.

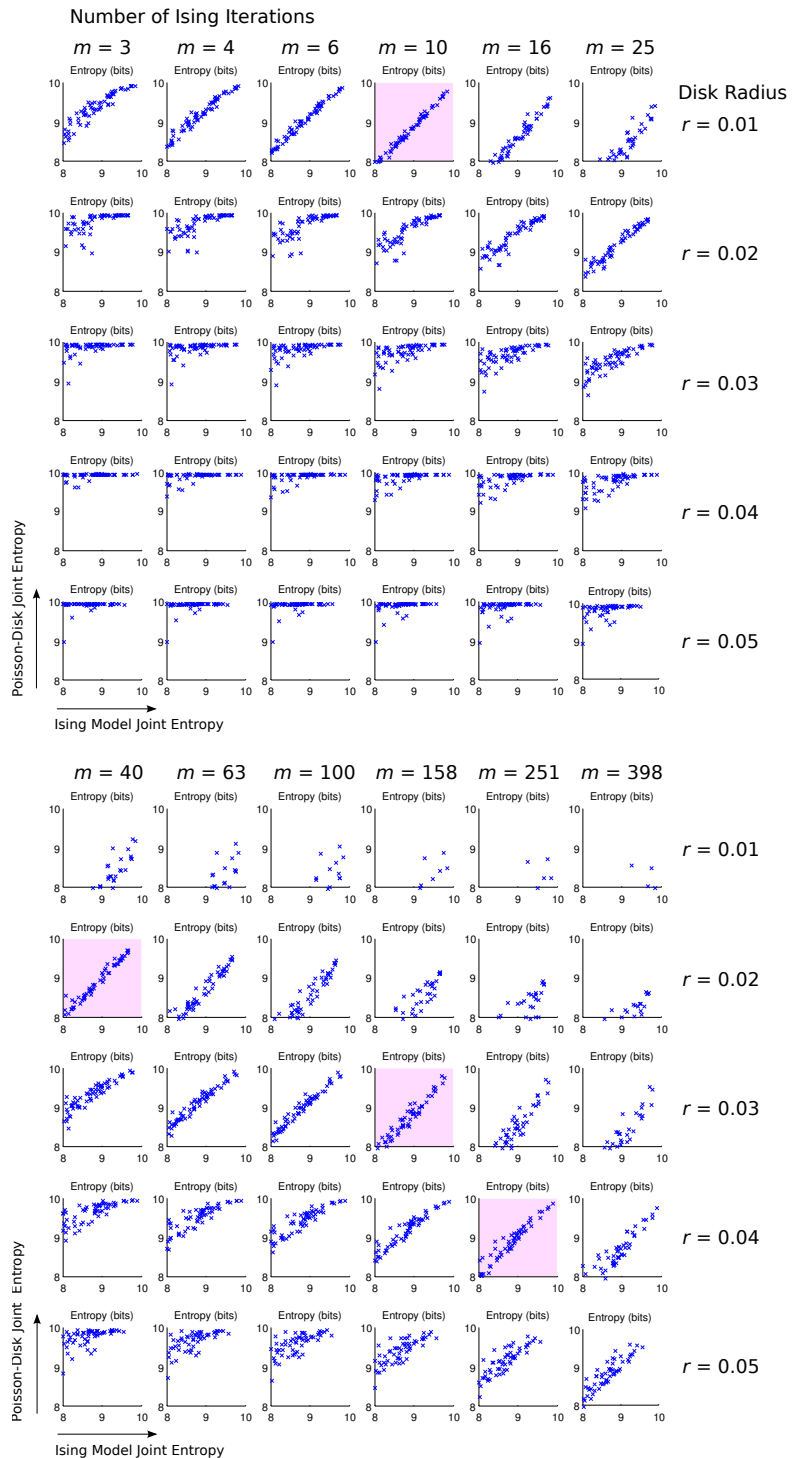


Figure 13: *Entropy Comparisons*

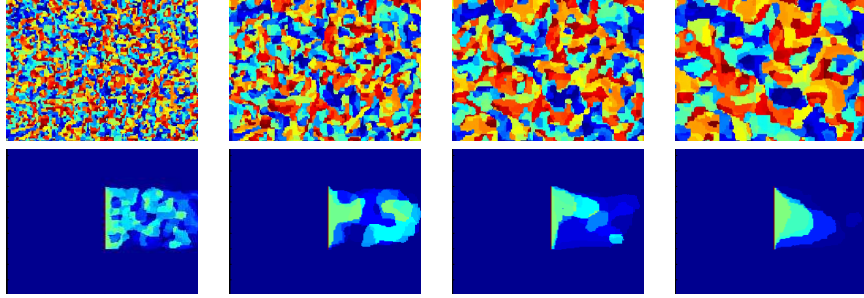


Figure 14: *Bit-Parallel Computation of Ising Marginal* “Bit twiddling” allows us to compute 64 simultaneous realizations of the Ising process on a single array of long integers. In the plots above, color is assigned according to nominal integer value, i.e. each realization contributes according to the significance of its bit position. This is the most direct way of visualizing the data, and the exponential decay of bit significance gives a sense of transparency and depth. Cf. Fig. 5.2.2

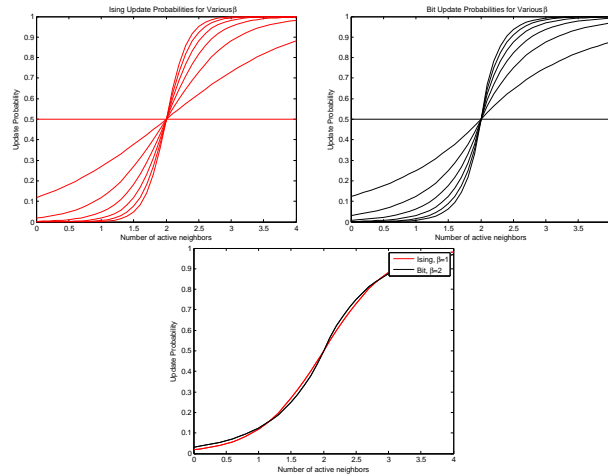


Figure 15: *Comparison of Update Probabilities*: Values of $\bar{\beta}$ are taken from 0 to 6. Update probabilities for the Ising Model and the parallel bit estimate are computed on the continuum $[0, 4]$, although only integers $\{0, \dots, 4\}$ are used in practice.

Observe that

$$\begin{aligned}
L^k &= (L^{k-1} \wedge (L^{k-1} \ll 2^{k-1})) \ll 3 \cdot 2^{k-1} - 2 \\
&= (L^{k-1} \ll 2^{k-1}) \wedge (L^{k-1} \ll 2 \cdot 2^{k-1}) \ll 2^k - 2 \\
&= (L^{k-1} \ll 2^{k-2}) \wedge (L^{k-2} \ll 2 \cdot 2^{k-2}) \\
&\quad \wedge (L^{k-1} \ll 3 \cdot 2^{k-2}) \wedge (L^{k-2} \ll 4 \cdot 2^{k-2}) \ll 2^k - 2 \\
&\quad \vdots \\
&= \left(\bigwedge_{j=0}^{2^k-1} (L^0 \ll j) \right) \ll 2^k - 1.
\end{aligned}$$

Thus, for the i -th bit of L^k :

$$(L^k)_i = \bigwedge_{j=2^k-1}^{2^{k+1}-2} L_{i-j}^0$$

where bit indices are taken modulo N . This is a 2^k -fold conjunction of independent random bits, so

$$P((L^k)_i = 1) = 2^{-2^k},$$

Observe, also, that the bits

$$(L^{k_1})_i = \bigwedge_{j=2^k-1}^{2^{k+1}-2} L_{i-j}^0 \quad \text{and} \quad (L^{k_2})_i = \bigwedge_{j=2^k-1}^{2^{k+1}-2} L_{i-j}^0$$

are independent for $k_1 \neq k_2$ (the ranges $[2^{k_1}-1, 2^{k_1+1}-2]$ and $[2^{k_2}-1, 2^{k_2+1}-2]$ do not overlap). Note, however that when indices i_1 and i_2 differ by less than 2^k , the bits $(L^k)_{i_1}$ and $(L^k)_{i_2}$ are highly correlated, especially for large k .

In modern processors, the bit-shift operation runs in constant time, so the random lookup integers $\{L^k, \dots, L^k\}$ are generated in $O(K)$ time.

7 Exploration

Having the range detector measurements (the observations) available $\mathcal{Y}(x_i) \in \mathcal{Y}$ at time t_i , we estimate $p_t(x)$ for a regular sampling of points in \mathcal{A}_t . Our next waypoint x_{t+1} is selected as

$$x_{t+1} = \arg \max_{x \in \mathcal{A}} E_t(x) \tag{17}$$

Exploration terminates when $E_t(x)$ falls below a certain threshold for all points on the sample grid.

7.1 Performance Bounds

These bounds depend on some conjectured properties of the Ising-model marginal visibility probabilities $p_t(x) = \mathbb{P}_t[x \in \mathcal{V}]$. Assume a fixed scaled-iteration-number $\mu := m/\text{scale}(m)$, and sufficiently-small grid spacings in G :

Conjecture 7.1 (Bounded Curvature of p_t). For any threshold $\epsilon > 0$, there is a finite constant $K = K(\epsilon)$, independent of \mathcal{V}_t and \mathcal{O}_t , such that (some suitable discrete analogue of) the boundary curvature of the level set $\{x : p_t(x) \leq 1 - \epsilon\}$ is bounded above by K .

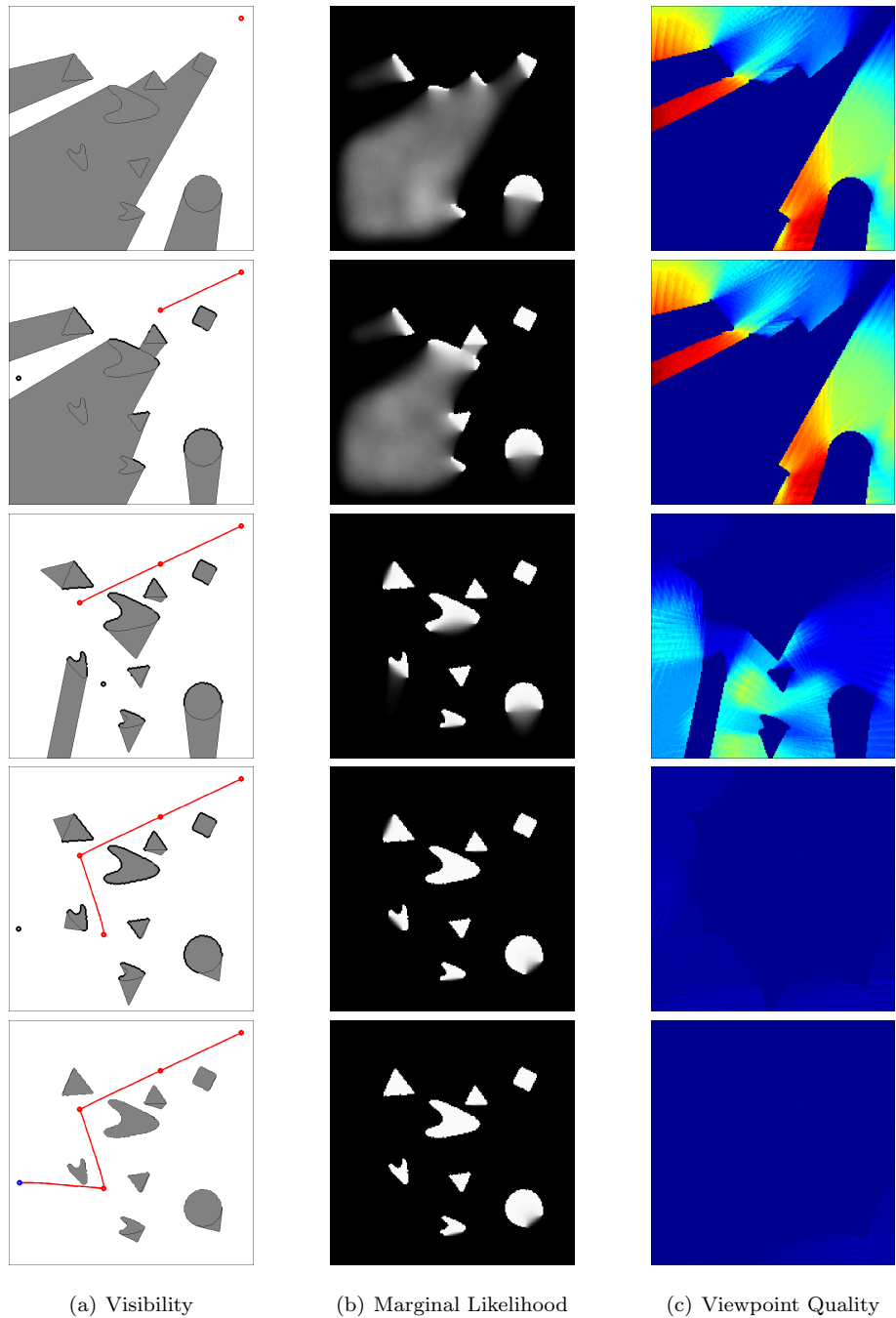
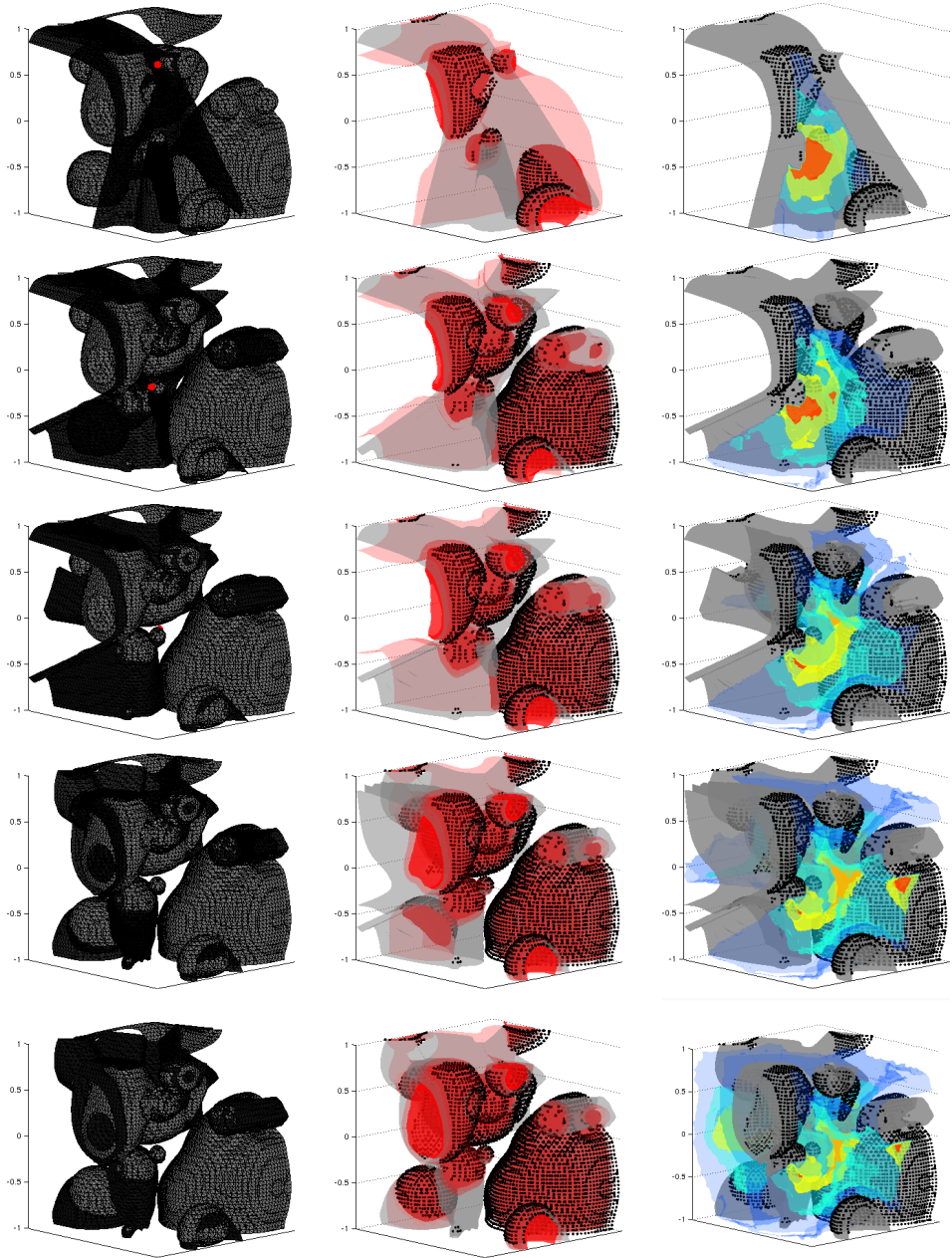


Figure 16: *Exploration of a 2D Scene* An explorer (red dot) attempts to efficiently map an unknown scene (a) by greedily choosing informative viewpoints (c). Observe that we are not merely uncovering area. Once the disposition of a site has been determined with high confidence (b), that site loses its informative value.



(a) Visibility

(b) Marginal Likelihood

(c) Viewpoint Quality

The result in ?, that the zero-temperature Ising model acts (in the scaling limit) as a curve-shortening flow on the level curves of binary images, suggests that the iterative low-temperature simulations that generate our hypothetical scenes will produce predictably-rounded hypothetical obstacles. In turn, it suggests that their pointwise average will have predictably-rounded level curves.

Now, let \mathcal{V}_t^r be the set of points in \mathcal{V}_t that lie at distance r or greater from points in \mathcal{O}_t , and let $\mathcal{V}_t^r(x_0)$ be the path-component of \mathcal{V}_t^r containing x_0 . Next, we make a sort of equicontinuity assumption:

Conjecture 7.2. For p sufficiently close to 1, and radius $r > 0$, there is a second radius $0 < r' \leq r$, independent of \mathcal{V}_t and \mathcal{O}_t , such that

$$(x \in \mathcal{V}_t^r \wedge p_t(x) > p \wedge d(x, z) < r') \\ \text{implies that } p_t(z) \geq \frac{1}{2}.$$

This would guarantee all points sufficiently far from known obstacles, with sufficiently high marginal probability, lie within disks of high marginal probability. These conjectures, if true, imply the following:

Lemma 7.1. Given a probability threshold $p_{\text{thresh}} > 0$, and radius r , there is an energy threshold $E_{\text{thresh}} > 0$ such that any point $x \in \mathcal{V}_t^r$ with $p_t(x) > p_{\text{thresh}}$ will induce an energy $E_t(y) > E_{\text{thresh}}$ at a nearby point y .

Proof: Let r' be as described in Conjecture 7.1, where r and p_{thresh} take the place of r and p . Then let

$$E_{\text{thresh}} = 2^{-\lambda r'/2} \pi \min \left\{ K(p_{\text{thresh}})^{-2}, \frac{1}{4} r'^2 \right\} \\ \cdot (-\log p_{\text{thresh}}).$$

Each of the three terms on the RHS is a lower bound of the corresponding term in the energy calculation, centered at x . The first bounds the area of the intersection between the level set $\{x : p_t(x) > p_{\text{thresh}}\}$ and the disk of radius r' , centered at x . For points z in this region, $\frac{1}{2} \leq p_t(z) \leq p_{\text{thresh}}$, and so

$$2^{-\lambda r'/2} \leq \exp \left(\lambda \int_0^{r'} \log p_t(z(s)) ds \right)$$

and

$$-\log p_{\text{thresh}} \leq -\log p_t(z) - (1 - p_t^{\lambda \beta s}(z)) \log(1 - p_t(z)).$$

□

Now, define

$$f(p, \beta, \lambda) = -\log(p_t(z)) - (1 - p_t^{\lambda \beta s}(z)) \log(1 - p_t(z))$$

$$M(\beta, \lambda) = \sup_{p: [0, \infty) \rightarrow [0, 1]} \int_{t=0}^{\infty} f(p(t), \beta, \lambda) \\ \exp \left(\lambda \int_{u=0}^t \log p(u) du \right) dt. \quad (18)$$

A restarting argument can be used to show that (18) is maximised by a constant function $p(t) = a$, so

$$M(\beta, \lambda) = \sup_a f(a, \beta, \lambda) \int_{t=0}^{\infty} \exp(\lambda t \log a) dt \quad (19)$$

$$= \sup_a \frac{f(a, \beta, \lambda)}{\lambda \log a}. \quad (20)$$

The last expression is continuous with respect to a , and bounded as $a \rightarrow 0$ and $a \rightarrow 1$, so $M(\beta, \lambda)$ does indeed exist.

Lemma 7.2. If an explorer has visited $y \in \mathcal{V}_t^r(x_0)$ before time t , then $E_t(y') < E_{\text{thresh}}$ for all points y' within distance $\delta = \delta(E_{\text{thresh}}, r, \beta, \lambda)$ of y , where $\delta = r \sin(\alpha/n_{\text{sh}})$, $\alpha = E_{\text{thresh}}/M(\beta, \lambda)$, and n_{sh} is the maximum number of disjoint shadow boundaries cast from a single point.

Proof: Traveling a distance δ in any direction will reveal a sliver of at most α along any shadow boundary. The maximum energy of such a vantage point is thus $n_{\text{sh}} \alpha M(\beta, \lambda)$.

□

Combining these two lemmas we get

Proposition 7.1. If A is the area of $\mathcal{V}^r(x_0)$, then, the greedy algorithm will take at most $A/\pi\delta(E_{\text{thresh}}r, \beta, \lambda)^2$ steps to bring $p_t(x)$ below p_{thresh} , for all points $x \in V^r(x_0)$.

7.2 Exploration Results

Using the exploration testbed provided by the authors of ?, we were able to compare our algorithm with theirs, in terms of (1) number of planning steps (2) total distance traveled by the explorer (3) unexplored area vs. total distance traveled, and (4) unexplored area at termination. Results are shown in Figure 17.

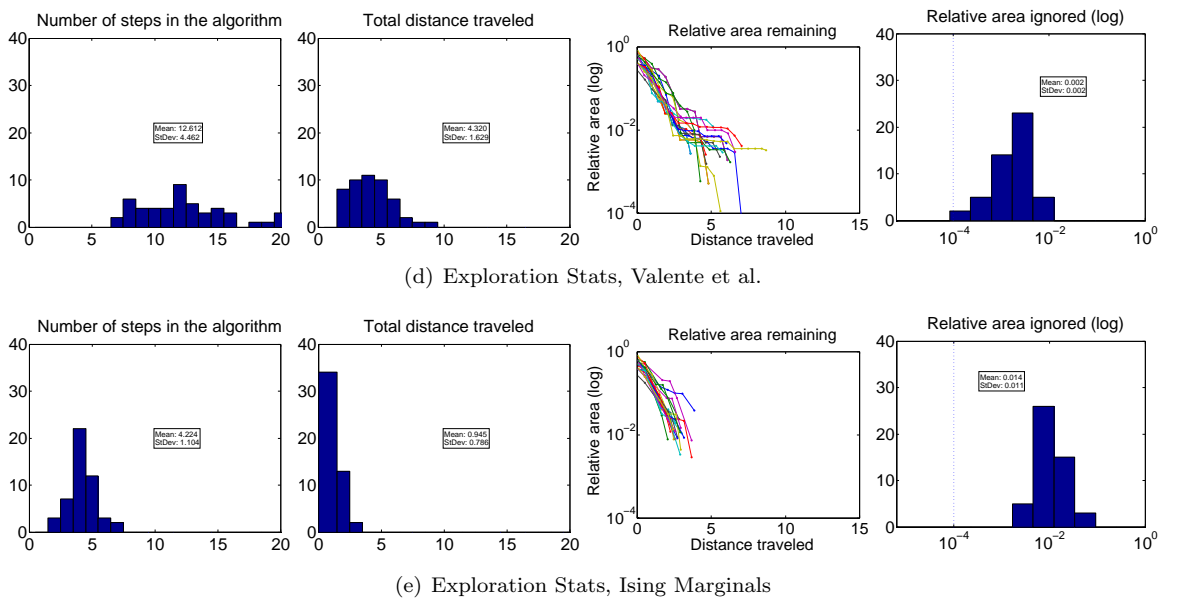


Figure 17: Exploration comparison with Valente et al.